Revisiting the link between extreme sea levels and climate variability using a spline-based non-stationary extreme value analysis

Jérémy Rohmer, Rémi Thiéblemont, Gonéri Le Cozannet

Weather and Climate Extremes 33 (2021) 100352

Contents lists available at ScienceDirect

Weather and Climate Extremes

journal homepage: www.elsevier.com/locate/wace

Revisiting the link between extreme sea levels and climate variability using a spline-based non-stationary extreme value analysis

Jérémy Rohmer *, Rémi Thieblemont, Gonéri Le Cozannet

BRGM, 3 Av. C. Guillemin, 45060, Orléans Cedex 2, France

ARTICLE INFO

Keywords:
Extremes
Climate indices
Non-stationary generalized extreme value distribution

ABSTRACT

Non-stationary extreme value analysis is a powerful framework to address the problem of time evolution of extremes and its link to climate variability as measured by different climate indices *CI* (like North Atlantic Oscillation NAO index). To model extreme sea levels (ESLs), a widely-used tool is the non-stationary Generalized Extreme Value distribution (GEV) where the parameters (location, scale and shape) are allowed to vary as a function of some covariates like the month-of-year or some *CIs*. A commonly used assumption is that only a few *CIs* impact the GEV parameters by using a linear model, and most of the time by focusing on two GEV parameters (location or/and the scale parameter). In the present study, these assumptions are revisited by relying on a data-driven spline-based GEV fitting approach combined with a penalization procedure. This allows identifying the type (non- or linear) of the *CI* influence for any of the three GEV parameters directly from the data, and evaluating the significance of this relation, i.e. without making any a priori assumptions as it is traditionally done. This approach is applied to the monthly maxima of sea levels derived from eight of the longest (quasi century-long) tide gauge dataset (Brest, France; Cuxhaven, Germany; Gedser, Denmark; Halifax, Canada; Honolulu, US; Newlyn, UK; San Francisco, US; Stockholm, Sweden) and by accounting for four major *CIs* (the North Atlantic Oscillation, the Atlantic Multidecadal Oscillation, the Niño 1 + 2 and the Southern Oscillation indices). From this analysis, we show that: (1) the links between *CIs* and different parameters of a GEV distribution fitted to ESL data are most of the time linear, but some of them present significant non-linear shapes; (2) multiple *CIs* should be considered to predict ESLs, and (3) the *CI* influence of the GEV distribution is not limited to the location parameter. These results are useful to understand current modes of variability of ESLs, and ultimately to improve coastal resilience through more precise extreme water level assessments.

1. Introduction

Extreme sea level (ESL) events due to storm surges are prominent threats for populations and ecosystems at the coasts, and their combination with mean sea level rise (MSL) are a major concern for coastal risk management and adaptation (Oppenheimer et al., 2019). Deepening our understanding of ESL drivers is of uttermost importance for emergency preparedness and design of early warning systems in order to improve anticipation of conditions leading to flooding (e.g., as outlined by Kundzewicz et al., 2019 for river flooding). Reliable estimates of return levels are key ingredients for coastal flood risk management (Nicholls and Cazenave, 2010). In this view, accounting for ESL distribution changes over time i.e. the non-stationary character of ESL, is critical as thoroughly discussed by Salas and Obeysekera (2014) regarding hydrological extremes, and by Cheng et al. (2014) in the context of changing climate.

In the present work, we are interested in the non-stationary character related to climate variability control, i.e. the links between ESL and climate oscillation patterns as measured by a range of climate variability indices (denoted *CIs*, like North Atlantic Oscillation (NAO) or Atlantic Multidecadal Oscillation (AMO)): a thorough understanding of these links could contribute to improving seasonal-to-decadal predictions (as shown for instance by Rashid and Wahl (2020) along the U.S. coastline), and potentially improving coastal flood hazard assessment (Muis et al., 2018) for both present day and for the future; in particular by reducing uncertainties in projections of extremes (e.g., Wong, 2018). In the context of climate change, a deeper knowledge of ESL drivers is a key element for the planning of adaptation strategies (like hard protection, managed realignment, retreat, etc.), for assessing the protective value of nature based solutions (e.g., sediment and dune management), and for

* Corresponding author.
E-mail address: j.rohmer@brgm.fr (J. Rohmer).

https://doi.org/10.1016/j.wace.2021.100352
Received 2 June 2020; Received in revised form 24 February 2021; Accepted 4 July 2021
Available online 6 July 2021

designing protective infrastructures (like dikes); see discussion by Wahl (2017). To appraise the significance of such projected changes, an improved understanding of the current variability of extreme sea level and its causes is thus needed.

Multidecadal changes in ESL have been recognized as mainly driven by variations in MSL, as extensively documented by many authors; (e.g. Menéndez and Woodworth, 2010; Woodworth et al., 2011; Wahl and Chambers, 2015, 2016; Frederikse et al., 2020; among others). In addition to MSL, forcing related to oscillations of the coupled ocean-atmosphere system (i.e. climate variability) can also impact ESL at different time scales ranging from inter-annual to multidecadal time scales (Han et al., 2019). To investigate such climate variability control, many studies use *CIs* see e.g., (Menéndez and Woodworth, 2010; Woodworth et al., 2011; Wahl and Chambers, 2015, 2016; Talke et al., 2014; Marcos et al., 2015; Mawdsley and Haigh, 2016; Marcos and Woodworth, 2017; Wong et al., 2018; Rohmer and Le Cozannet, 2019), among others.

In practices, the analysis of ESL and their return levels generally relies on Extreme Value Theory, which provides a rigorous framework (Coles, 2001), in particular by means of the widely-used Generalized Extreme Value (GEV) model whose cumulative distribution function holds as follows:

$$\begin{aligned}&\text{Probability}(SL \le sl)\\&= \exp\left(-\left(1+\xi\left(\frac{sl-\mu}{\sigma}\right)\right)_+^{-1/\xi}\right) \text{ with } \left(1+\xi\left(\frac{sl-\mu}{\sigma}\right)\right)_+\\&= \max\left(0, 1+\xi\left(\frac{sl-\mu}{\sigma}\right)\right)\end{aligned} \quad (1)$$

where sl is the sea level measured at tide gauges; μ, $\sigma>0$ and $\xi\neq$ are the GEV location, scale, and shape parameters, respectively.

Fig. 1 illustrates the behavior of the GEV cumulative probability distribution depending on the value of the GEV parameters. In particular, the GEV distribution presents an asymptotic horizontal behavior for $\xi < 0$ (i.e. the asymptotically–bounded distribution, which corresponds to the Weibull distribution); unbounded when $\xi > 0$ (i.e. high probability of occurrence of great values can be reached, which corresponds to the Fréchet distribution); and intermediate in the case of $\xi = 0$ (Gumbel distribution, as a limiting case of Eq. (1)). Fig. 1b and c respectively shows that the location parameter μ primarily translates the whole probability distribution, while the scale primarily affects the dispersion of the distribution.

To study the climate variability control on *ESL*, an efficient approach relies on the non-stationary formulation of GEV, i.e. a GEV distribution, whose parameters are allowed to vary as a function of some time-varying covariates, like the month-of-year to account for seasonality (denoted *moy*) or some *CIs* to account for large-scale climate variability. The focus of the current study is the modelling of the influence of *CIs* on the GEV parameters. To do so, the use of the linear model is a common practice. For instance, Méndez et al. (2007) focused on the linear link between sea level and Southern Oscillation indices (SOI) at San Francisco; Menéndez and Woodworth (2010) analyzed the linear relationships with different *CIs* using tide gauge datasets from the GESLA tide gauge data repository (Woodworth et al., 2016); Marcos and Woodworth (2017) examined spatiotemporal changes in extreme sea levels along the coasts of the North Atlantic and the Gulf of Mexico with similar techniques; Grinsted et al. (2013) examined the risk of hurricane-induced surges using similar techniques; Ceres et al. (2017) and Cheng et al. (2014) included a simple linear link with time as the covariate. Besides, the analysis is often restricted to μ; some studies examine the linear dependence for the logarithm of σ as well, but the control on ξ of time-varying covariates (and more particularly of *CIs*) is only rarely investigated.

In this study, we propose to re-examine the commonly-used assumptions for investigating the evolution of ESL. More specifically, we aim at addressing the following research questions: (Q1) Is the non-stationary GEV with linear model adequate? (Q2) Can multiple *CIs* influence ESL? (Q3) Is the influence only on μ or is there any influence on the other GEV parameters? To do so, we propose to rely on a data-driven fitting approach within the general framework of Generalized Additive Model for Location, Scale and Shape parameter (GAMLSS; e.g., Rigby and Stasinopoulos, 2005) to identify whether a (statistically) significant relation exists for any of the GEV parameters.

The paper is organized as follows. In Sect. 2, we describe the sea level records, their processing to extract extremes, and the considered large-scale *CIs*. In Sect. 3, further details are provided on the fitting of the non-stationary GEV distribution within the GAMLSS framework. In Sect. 4, we first apply the fitting procedure to the specific tide gauge of Cuxhaven (Germany). Then, we investigate the *CI* contribution on a larger set of tide gauges worldwide. Finally, we discuss the results in Sect. 5.

2. Data

We use the data from the Global Extreme Sea Level Analysis (GESLA, version 2, Woodworth et al., 2016) tide gauge data repository, and focus on eight of the longest (quasi century-long) time series of SL sampled at an hourly frequency, namely: Brest, France (1871–2013); Cuxhaven, Germany (1918–2014); Gedser, Denmark (1892–2012); Halifax, Canada (1920–2011); Honolulu, US (1905–2012); Newlyn, UK (1916–2014); San Francisco, US (1898–2012); Stockholm, Sweden (1889–2012). A pre-processing has been applied to restrict the analysis to the subsets of the timeseries where the data only present limited missing values over a continuous time duration not longer than 10 years.

We then process the hourly *SL* data by extracting the monthly maxima *MM*. Since we are interested in the climate variability control on *ESL* over and above changes in *MSL*, we follow the approach by

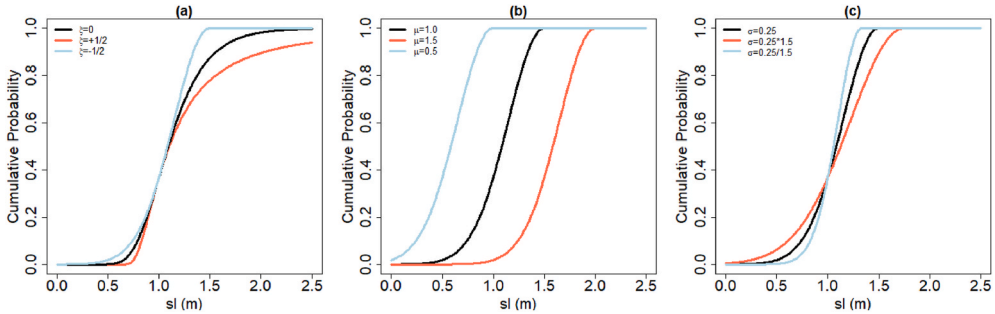

Fig. 1. Behavior of the GEV cumulative probability distributions depending on the changes in the parameter value: (a) ξ (with μ fixed at 1.0, and σ fixed at 0.25); (b) μ (with ξ fixed at −0.5, and σ fixed at 0.25); (c) σ (with μ fixed at 1.0, and ξ fixed at 0.5).

Menéndez and Woodworth (2010), and remove the effect of *MSL* by subtracting the annual median of the hourly values. The processed data are denoted *rMM*. The time series of the corresponding data are provided in Fig. 2.

We focus on four major CIs that are widely used as predictors in the study of ESLs: the North Atlantic Oscillation (NAO), the Atlantic Multidecadal Oscillation (AMO – smoothed version), the Niño 1 + 2 (NINO12) and the Southern Oscillation (SOI) indices. NAO is the dominant mode of winter climate variability in the Northern Atlantic sector (Hurrell et al., 2003) and is defined as the normalized pressure difference between the Azores and Iceland (https://www.esrl.noaa.gov/psd/gcos_wgsp/Timeseries/NAO/). NAO has been shown to influence significantly sea level variability along the North Atlantic, Baltic or Mediterranean coasts at various timescales (e.g. Calafat et al., 2012; Chafik et al., 2017). AMO (https://www.esrl.noaa.gov/psd/gcos_wgsp/Timeseries/AMO/) measures alternating warm and cool phases of the North Atlantic sea-surface temperature on multi-decadal timescale (i.e. ~60–80 years) and can also affect sea level in the North Atlantic (see e.g. Xu et al., 2019; Han et al., 2017 and reference therein). In the Pacific basin, El Niño–Southern Oscillation (ENSO) has been demonstrated to have a significant influence on coastal sea-level variability (e.g. Merrifield et al., 1999; Chang et al., 2013). Here, we relied on SOI (https://psl.noaa.gov/gcos_wgsp/Timeseries/SOI/) and Niño 1 + 2 (https://www.psl.noaa.gov/gcos_wgsp/Timeseries/Nino12/) indices to characterize climate variability in the tropical Pacific. In our study, climate indices are derived either from station-based sea-level pressure records (NAO, SOI) or observational reconstruction of sea surface temperature (AMO, Niño 1 + 2) and allow tracking climate variations, jointly for the four indices, back to 1870's. Finally, note that their absolute pairwise correlation (Pearson, Spearman, Kendall) are small-to-moderate (not larger than 10% for NAO, AMO and NINO12, and at maximum ~40% for SOI and NINO12); see also the matrix of pairwise correlation coefficients in Supplementary Material C.

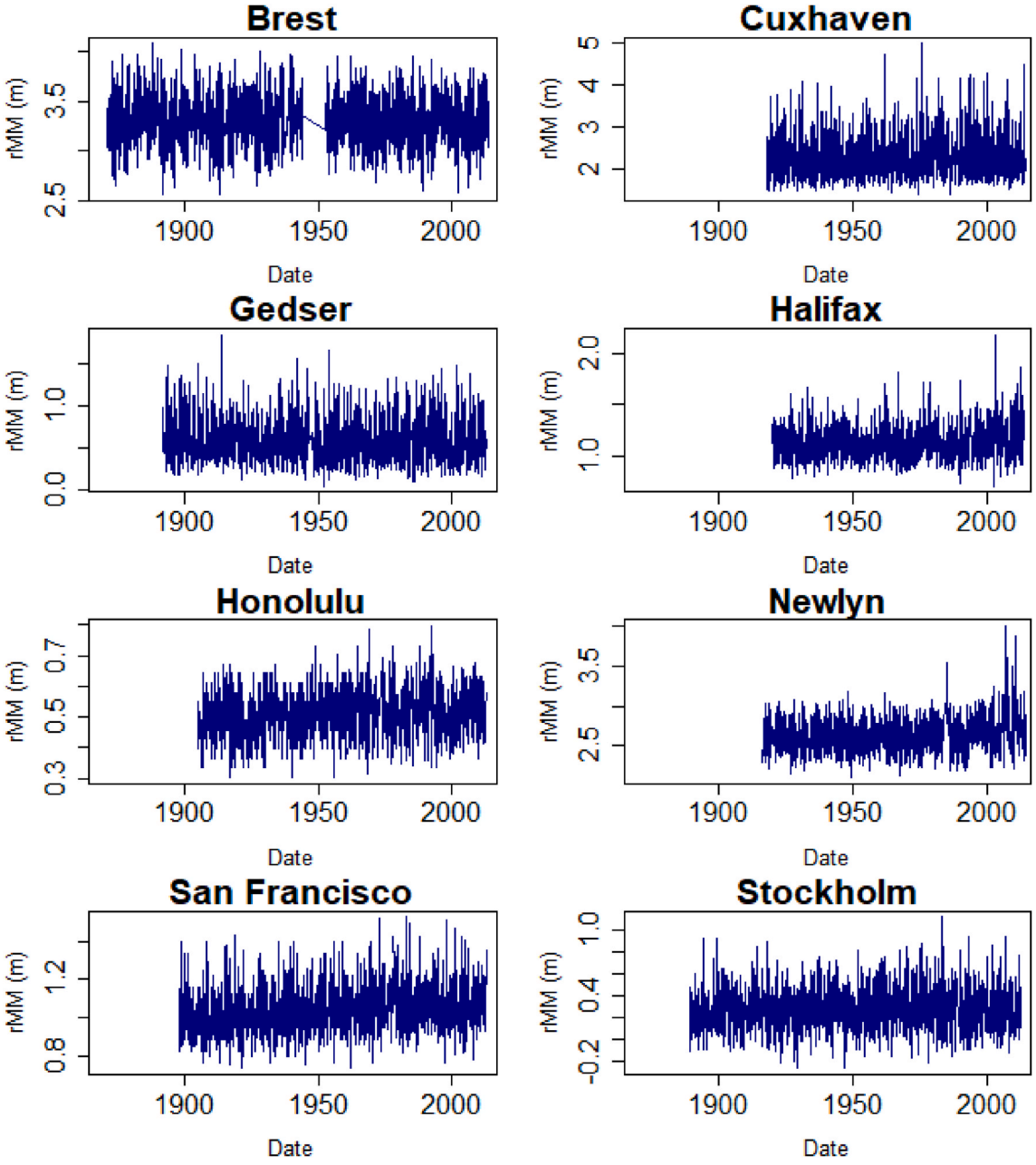

Fig. 2. Time series of monthly maxima *rMM* of sea levels (with removed MSL) for the eight tide gauges considered in the current study.

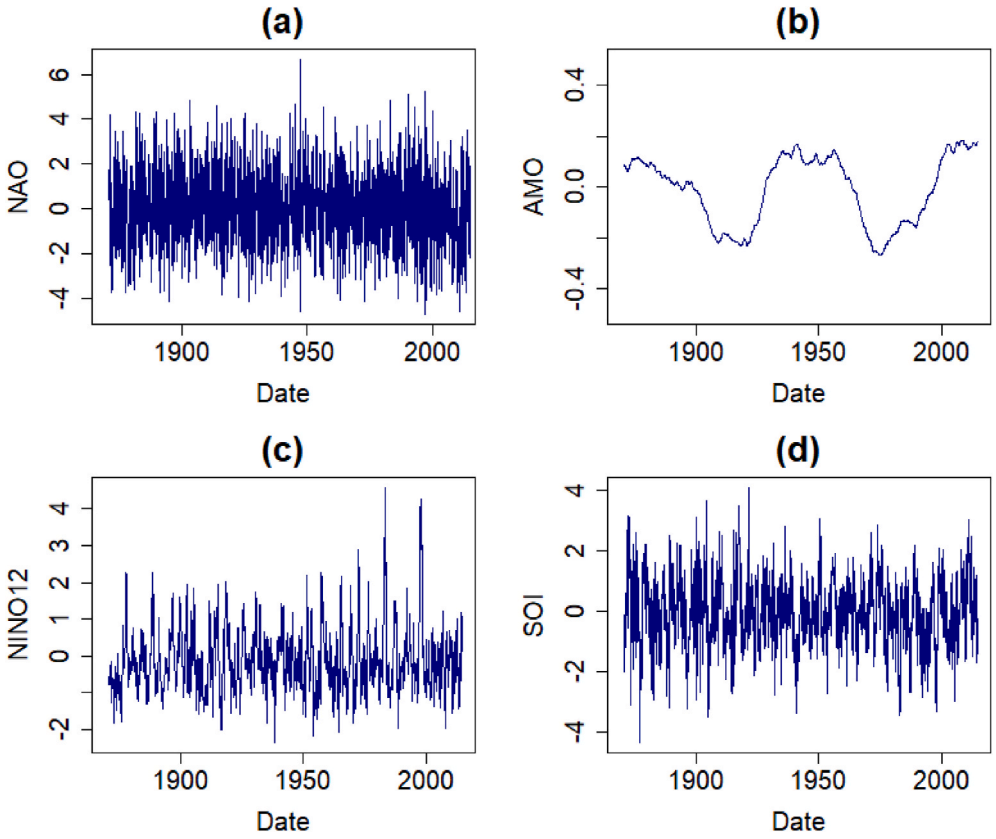

Fig. 3. Monthly time series of Climate Indices considered in the study, namely NAO (a), AMO (b), NINO12 (c), and SOI (d).

3. Statistical methods

3.1. Overall procedure

To model the monthly sea level maxima *rMM* (with removed effect of *MSL* as described in Sect. 2), we consider three different non-stationary GEV formulations (see a formal presentation in Sect. 3.2). GEV1 for which only the location parameter is a function of the covariates, GEV2 for which both location and scale parameters are functions of the covariates, and GEV3 when the three GEV parameters are functions of the covariates. The covariates are the *CIs* selected in Sect. 2. To answer the afore-described research questions regarding the effect of *CIs*, we implement different statistical methods:

- To answer Q1 (is the linear model adequate?), the mathematical relation (named partial effect) between the GEV parameters and the *CIs* is learnt from the data using the non-parametric GAM models (see implementation details in Sect. 3.2). The partial effect is then used to assess the influence on the different GEV parameters;
- To answer Q2 (can multiple *CI* influence extremes?), the fitting procedure is completed by a penalization procedure that selects the most important covariates during model construction (Sect. 3.3);
- To answer Q3 (is the influence only on μ or is there any influence on the other GEV parameters?), we select the most appropriate model among the three GEV1,2,3 formulations using information criteria (Sect. 3.4).

Finally, the goodness of fit of the selected model is evaluated by means of diagnostic analysis based on quantile-quantile and probability-probability plots described in Sect. 3.5.

In addition to the *CI* effect, seasonal and an inter-annual effects are included by considering the month-of-year (*moy*), and the considered year (*YY*) as covariates. Evidences for an inter-annual memory in mean sea-level changes have been identified and mostly related to the spatial and time variability of sea-level changes (Dangendorf et al., 2014; Becker et al., 2014), and similar effects are affecting ESLs and more particularly some specific parameter of the GEV distribution, as exemplified by Menéndez and Woodworth (2010) globally; see also an example by Méndez et al. (2007) at San Francisco.

3.2. Non-stationary GEV

The GEV distribution is assumed to be non-stationary in the sense that the GEV parameters $\boldsymbol{\theta}=(\mu,\sigma,\xi)$ vary as a function of the covariates *moy*, *YY*, and $\boldsymbol{x} = CI$ (described in Sect. 2). Since the scale parameter satisfies $\sigma > 0$, we preferably work with its log-transformation. Computing non-stationary GEV models with varying shape parameter is known to be difficult, and might lead to unstable results. To minimize this problem, we work with a modified logit transformation of ξ (restricting its range to -1 to 0.5) by following the implementation provided in the *mgcv* R package (Wood, 2017: chapter 7).

We assume that the model $\eta_\theta(.)$ linking $\boldsymbol{\theta}$ to the covariates can be decomposed into three functional terms as follows:

$$\eta_\theta(YY, moy, \boldsymbol{x}) = \eta_\theta^{LT}(YY) + \eta_\theta^{\text{seasonal}}(moy) + \eta_\theta^{CI}(\boldsymbol{x}) \quad (2)$$

where $\eta_\theta^{LT}(.)$ is long term trend; $\eta_\theta^{seasonal}(.)$ is a seasonal term related to *moy*, and $\eta_\theta^{CI}(.)$ is the term related to the climate variability control.

To account for the effect of *YY* and of *moy*, we follow the approach by Menéndez and Woodworth (2010) by modelling η_θ^{LT} as a linear model with respect to *YY* and by modelling $\eta_\theta^{seasonal}(.)$ as a summation of sinusoidal functions with respect to *moy* as follows:

$$\eta_\theta^{seasonal}(moy) = \beta_0 + \sum_{i=1}^{2} \beta_{2i-1}.\cos(i.\omega.moy) + \beta_{2i}.\sin(i.\omega.moy) \quad (3)$$

where $\boldsymbol{\beta}$ are the regression coefficients, and $\omega = 2\pi/12$.

To account for the effect of *CIs*, we rely on the general framework of Generalized Additive Model for Location, Scale and Shape parameter (GAMLSS; e.g., Rigby and Stasinopoulos, 2005). Contrary to most existing studies, we aim at keeping the learning process of the mathematical relation between $\boldsymbol{\theta}$ and *CI* as generic as possible by:

- Avoiding the introduction of a priori regression models like linear or polynomial;
- Identifying whether a significant relation exists for any of the three GEV parameters;
- Selecting the most important covariates during the fitting process.

To do so, we rely on a data-driven spline-based regression approach by assuming that the model $\eta_\theta^{CI}(.)$ linking $\boldsymbol{\theta}$ to *CI* follows a semi-parametric additive formulation as follows:

$$\eta_\theta^{CI}(\boldsymbol{x}) = \sum_{j=1}^{J} f_j(x_j) \tag{4}$$

where J is the number of functional terms that is generally less than the number of input variables, $f_j(.)$ corresponds to a univariate smooth non-linear model described as follows:

$$f_j(x) = \sum_b \beta_{jb} b_b(x) \tag{5}$$

with $b_b(.)$ the thin plate spline basis function (Wood, 2003) and with additional penalties on the regression coefficients β_{jb} for smoothness.

The functional terms in Eq. (4) are termed as "partial effect" and hold the information of each covariate's individual effect on the considered GEV parameter. The interest is to model the mathematical relationship between each GEV parameter and the covariate in a flexible manner, i.e. by avoiding at maximum the introduction of assumptions on the form/shape of this relationship.

The model estimation consists in evaluating the regression coefficients $\boldsymbol{\beta}$ (associated to the GEV parameters $\boldsymbol{\theta}$) by maximizing the log-likelihood $l(.)$ of the GEV distribution. To avoid overfitting, the estimation is based on the penalized version of $l(.)$ to control the roughness of the smooth functional terms (hence their complexity) by solving:

$$\underset{\beta}{\operatorname{argmax}} \left(l(\boldsymbol{\beta}) - \frac{1}{2} \sum_j \lambda_j \boldsymbol{\beta}^T \boldsymbol{S}_j \boldsymbol{\beta} \right) \tag{6}$$

where λ_j control the extent of the penalization (i.e. the trade-off between goodness-of-fit and smoothness), and $\boldsymbol{S}_j$ is a matrix of known coefficients (such that the terms in the summation measure the roughness of the smooth functions). Computational methods and implementation details are described in Wood et al. (2016) and references therein. In the present study, we choose a selection of the penalization term via minimization of the generalized cross-validation criterion.

3.3. Variable selection

The introduction of the penalization coefficients in Equation (6) has two effects: they control how variable and smooth the function is (i.e. smoothing effect) and they can penalize the absolute size of the function (i.e. shrinkage effect) as discussed by Marra and Wood (2011). The second effect is of high interest to screen out input variables of negligible influence. However, the penalty is known to have a limited action, since the formulation of Equation (6) can only affect the components that have derivatives, i.e. the "range space" of a spline basis, which corresponds to the space of smooth non-linear functions. Yet this does not affect the other parts, i.e. the "null space", which corresponds to the space of "completely smooth functions" that includes constant or linear functions. For an univariate thin plate regression spline, this means that there is a linear term left in the model, even when the penalty value is very large (as $\lambda \to \infty$), and the afore-described procedure does not ensure that a covariate of negligible influence will completely be filtered out by the analysis (with corresponding regression coefficient shrunk to zero). In this situation, this means that the resulting partial effect might still present a low magnitude signal.

To deal with this problem, we rely on the approach termed as "shrinkage" described in Marra and Wood (2011): Sect. 2.2. Let us consider the decomposition of $\boldsymbol{S}_j$:

$$\boldsymbol{S}_j = \boldsymbol{U}_j \boldsymbol{\Lambda}_j \boldsymbol{U}_j^T \tag{7}$$

where $\boldsymbol{U}_j$ is an eigenvector matrix associated with the jth smooth function, and $\boldsymbol{\Lambda}_j$ is the corresponding diagonal eigenvalue matrix.

The presence of zero eigenvalues in $\boldsymbol{\Lambda}_j$ is at the origin of the afore-described problem. A possible solution is to set up them to a constant value ε corresponding to a small proportion of the smallest strictly positive penalty eigenvalues of $\boldsymbol{S}_j$, so that, for large enough smoothing parameters, the smooth becomes identically zero. This allows automatic smoothing parameter selection methods to effectively remove the term from the model.

3.4. Model selection

We select the most appropriate model among the three formulations GEV1,2,3 by analyzing information criteria as recommended for instance by Kim et al. (2017). We focus on the Akaike information criterion (AIC; Akaike, 1998), because we are interested in the predictive capability of the resulting model (contrary to the Bayesian information criterion (BIC; Schwarz, 1978), which preferably gives insights in goodness of fit, see e.g., Höge et al., 2018). AIC formulation holds as follows:

$$AIC = -2\,l + 2k \tag{8}$$

where k is the number of degree of freedoms of the model, $l(.)$ is the log-likelihood.

The most appropriate model is the one that minimizes the AIC criterion, i.e. the model with higher predictability but not too complex (i.e. without a too large number of parameters). Since the constructed models use penalization for the smoothness (Sect. 3.2), we rely on the formulation provided by Wood et al. (2016: Sect. 5) to account for the smoothing parameter uncertainty.

Yet, selecting the most appropriate model may not be straightforward in all situations when two model candidates present close AIC values. For instance, Burnham and Anderson (2004) suggests an AIC difference of at least 10 to be able to rank with confidence the most and the second most appropriate model. If this criterion is not met, we complement the analysis with the likelihood ratio test LRT (e.g., Méndez et al., 2007), which compares here two hierarchically nested GEV formulations using $L = -2(l_0\text{-}l_1)$, where l_0 is the maximized log-likelihood of the simpler model M_0 and l_1 is the one of the more complex model M_1 (that presents q additional parameters compared to M_0 and contains M_0 as a particular case). The criterion L follows a chi-squared distribution with q degrees of freedom, which allows deriving a p-value of the test.

3.5. Model checking

Once selected, some diagnostic information about the model fitting procedure can be performed by combining a transformation of the data to a Gumbel distributed random variable (e.g. Beirlant et al., 2004) and an analysis of the corresponding residual quantile and probability plot on Gumbel scale; see e.g. Méndez et al. (2007) for an example of application. If the model distributional assumptions are met then the considered plot should be close to a straight line. The visual analysis of the residual quantile plot is completed by a quantitative indicator

defined as follows:

$$Q^2 = 1 - \frac{\sum_{i=1}^{n}\left(q_i - \widehat{q}_i\right)^2}{\sum_{i=1}^{n}(q_i - \overline{q})^2} \quad (9)$$

where $\widehat{q}_i$ is the ith estimate of the theoretical quantile q_i and $\overline{q}$ is the average value calculated over all observations i = 1, …,n.

The Q^2 criterion also applies for the residual probability plot by replacing the theoretical quantile q_i by the theoretical probability. A coefficient Q^2 close to 1.0 indicates a satisfactory goodness of fit of the considered GEV. In the following, we focus on the evaluation of Q^2 for large values, i.e. quantile above 2, and probability above 80%.

4. Results

4.1. Application to Cuxhaven tide gauge

We apply the procedure described in Sect. 3.1 on the *rMM* data at Cuxhaven tide gauge. We consider the three GEV model's formulations described in Sect. 3.1. The corresponding AIC criterion values reach 1320, 1102, and 1107 for GEV1, 2, and 3 respectively. This indicates that GEV2 and GEV3 model are both identified as appropriate (the AIC difference is small). Thus, we complement this analysis with the LRT test, which shows a high p-value of 40% (i.e. well above the significance threshold of 1%) hence favouring the selection of the simpler model GEV2.

In addition, the residual quantile plot (Gumbel scale) in Fig. 4a shows a better agreement for the large Gumbel theoretical quantiles (here above 4) when considering GEV2. This provides a second element in favour of the GEV2 model. The analysis of the residual probability plot on Gumbel scale (Fig. 4b) shows however little differences between both models. Finally, the examination of the partial effects derived from the application of GEV3 for ξ clearly highlights the absence of *CI* influence (Supplementary Material A).

These elements suggest a non-stationary GEV model with fixed and constant shape parameter, here evaluated at 0.010 ($\pm$0.025), hence indicating a Gumbel type tail behaviour.

Using GEV2 model, we identify the contributions of the different covariates (*YY*, *moy* and *CIs*) by analysing the partial effects. The partial effect related to *YY* reveals a long term influence on μ with a statistically significant linear coefficient of $8.1e^{-4}$ ($\pm 3.1e^{-4}$), i.e. this indicates that despite the removal of the MSL effect (via the annual median value removal), an inter-annual effect still remains. The examination of the seasonal partial effects (related to *moy*) reveals a temporal evolution that is consistent with what is known from the storm activity in this region i.e. higher frequency of storms in winter season (see e.g. Lang and Mikolajewicz, 2019). This is outlined by maxima on the partial effects for December–January for both μ (Fig. 5a) and σ (Fig. 5b); hence showing that seasonality both influences the overall shift and the dispersion of the probability distribution (as illustrated in Fig. 1).

Figs. 6 and 7 provide the partial effects related to the climate indices. Fig. 6b shows a strong quasi-linear effect of NAO. This signal can be considered with high confidence, because the upper and lower bounds of the uncertainty band are consistent with the tendency provided by the best estimate (i.e. the uncertainty bands indicate positive (respectively negative) partial effects when the best estimate indicates it). In particular, it is interesting to note that this result is consistent with the study by Lang and Mikolajewicz (2019). The influence of AMO and of NINO12 is here identified as negligible (the partial effects are shrunk to zero using the approaches of Sect. 3.3). We also note a small-to-moderate linear signal of SOI. This partial effect should however be considered with cautious given the uncertainty band.

Fig. 7 complements this analysis for log(σ) and shows a strong linearly increasing signal of NAO as well. These results indicate that under increased positive NAO conditions, the ESL distribution is shifted toward higher extremes (Fig. 1b) and its spread tends to extend (Fig. 1c). NINO12 and SOI appear to influence log(σ), but the width of the uncertainty band (including the smoothing parameter uncertainty) is so large that the derived partial effect cannot be considered with confidence.

4.2. Analysis at multiple coastal sites

The procedure is now applied to all tide gauges. Table 1 provides the AIC value, which shows that GEV3 appears to be appropriate for Halifax, Honolulu, Newlyn, and Stockholm. The AIC-based selection for Brest, Cuxhaven, Gedser, and San Francisco is however more tedious (as indicated by very close values between GEV2 and GEV3). The LRT p-value (above the significance threshold of 1%) is then used and shows that the GEV2 model should be preferably selected for Brest, Cuxhaven, Gedser and San Francisco. The examination of the residual quantile (respectively probability) plot on Gumbel scale indicates satisfactory goodness of fit for large quantiles above 2 (respectively large probabilities above 80%) as shown by the satisfactory Q^2 indicator values >90% (Table 2).

Similarly to Cuxhaven, the influences of the *CIs* are analyzed by examining the corresponding partial effects. The long term as well as the season partial effects are reported in Supplementary Materials D and E. In particular, the seasonal evolutions appeared to be consistent with previous work on these effects (see e.g., Menéndez and Woodworth, 2010). Fig. 8 summarizes the different types of partial effects at each tide gauge considering the different climate indices and GEV parameters.

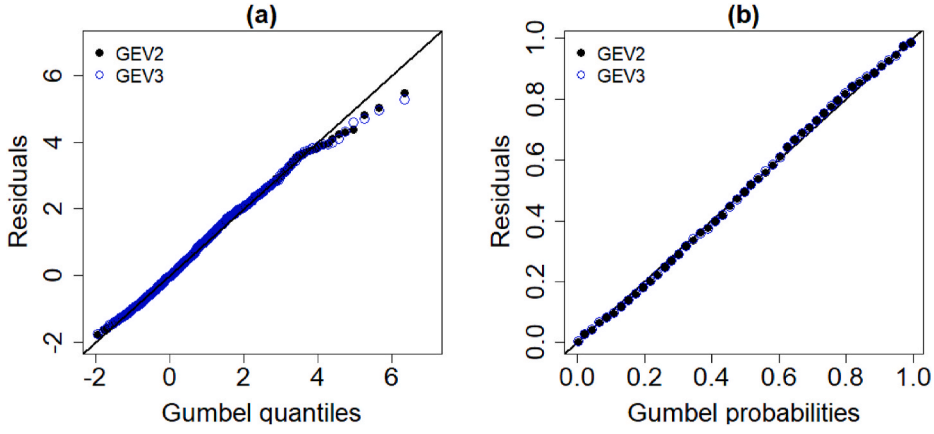

Fig. 4(a). Residual quantile plot on Gumbel scale for the GEV2 (black dots) and GEV3 (blue dots) model at Cuxhaven tide gauge; (b) Residual probability plot on Gumbel scale. (For interpretation of the references to colour in this figure legend, the reader is referred to the Web version of this article.)

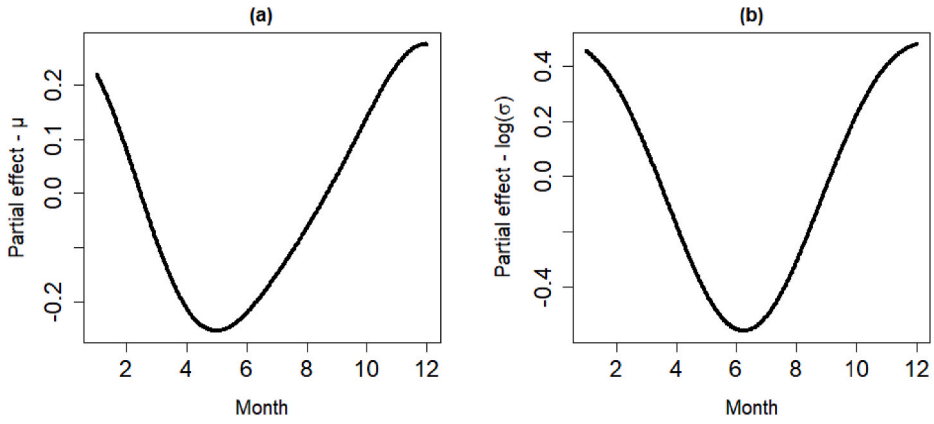

Fig. 5. Partial effects at Cuxhaven related to the month of the year for μ (a) and for $\log(\sigma)$ (b).

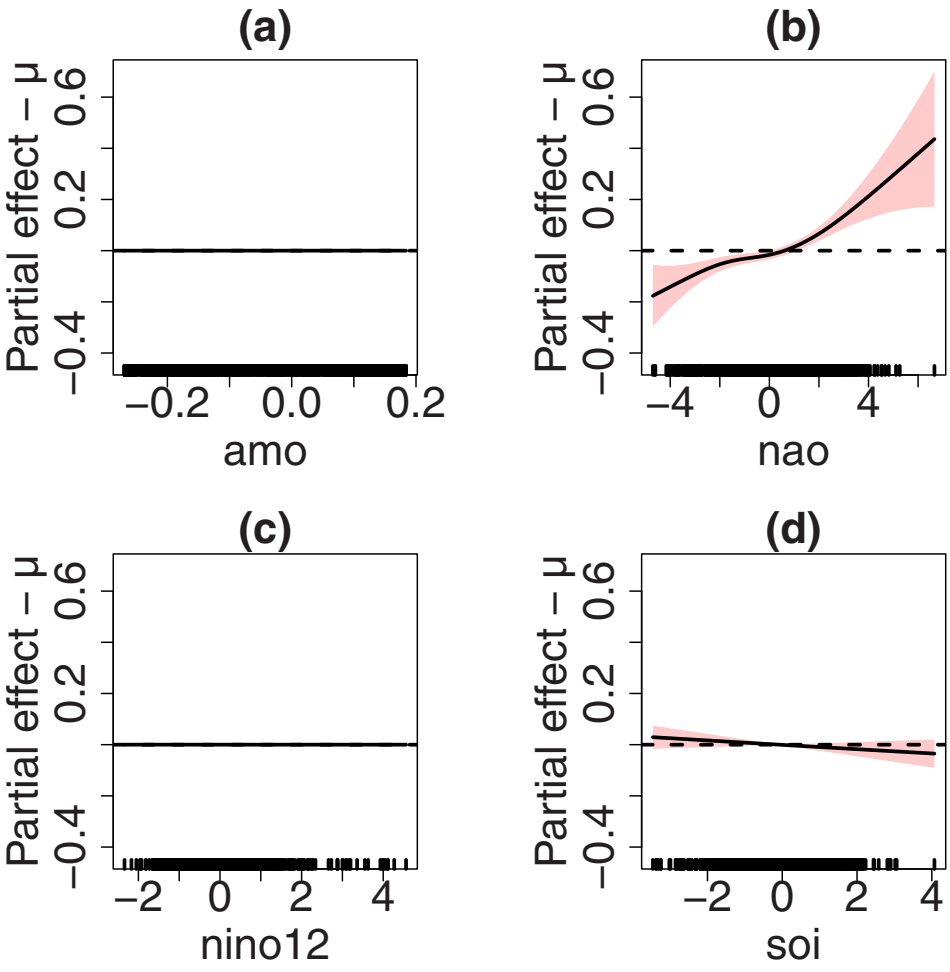

Fig. 6. Partial effects of μ (a–d) as function of the covariates at Cuxhaven. The red-coloured uncertainty envelope (including the smoothing parameter uncertainty) is defined by two standard errors above and below the best estimate (black line). Flat partial effects indicate an absence of influence of the considered covariate. (For interpretation of the references to colour in this figure legend, the reader is referred to the Web version of this article.)

When the upper and lower bound of the uncertainty band are not consistent with the tendency provided by the best estimate (i.e. the uncertainty bands indicate positive (respectively negative) partial effects when the best estimate indicates the contrary), this is indicated by a light colour.

Regarding research question Q1 (is the linear model adequate?), the partial effects related to *CIs* are mainly of linear type (either increasing or decreasing). Among the total number of partial effects (here of 20) identified with high confidence (i.e. with uncertainty band consistent with the best estimate marked by warm colours in Fig. 8), 13 are linear and concerns μ (six tide gauges), σ (six tide gauges) and ξ (one tide gauge). At Brest and Honolulu, only the seasonal and inter-annual effects are derived with high confidence (the *CI* effect are associated with too high uncertainty).

Though the linear assumption seems to be valid for most cases, there are statistically significant non-linear effects derived at four tide gauges

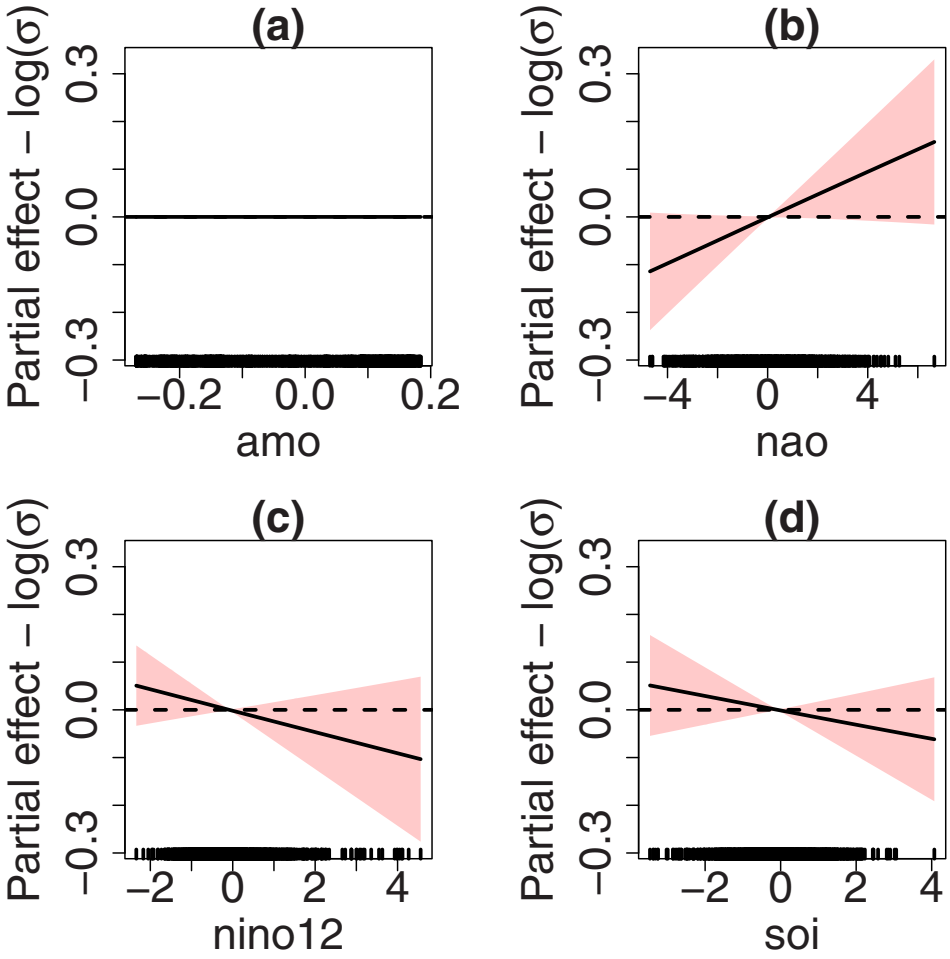

Fig. 7. Partial effects of log(σ) (a–d) as function of the covariates at Cuxhaven. The red-coloured uncertainty envelope (including the smoothing parameter uncertainty) is defined by two standard errors above and below the best estimate (black line). Flat partial effects indicate an absence of influence of the considered covariate. (For interpretation of the references to colour in this figure legend, the reader is referred to the Web version of this article.)

Table 1
Information criterion AIC evaluated for three formulations of the non-stationary GEV model. Bold numbers correspond to the minimum values. The p-value of the LRT is the one comparing GEV2 and GEV3.

Tide gauge	GEV1	GEV2	GEV3	LRT p-value
Brest	−438	**−476**	−470	41%
Cuxhaven	1320	**1102**	1107	47%
Gedser	−404	−719	**−720**	4.1%
Halifax	−1562	−1640	**−1659**	<1%
Honolulu	−3437	−3484	**−3510**	<1%
Newlyn	−524	−557	**−628**	<1%
San Francisco	−2522	**−2782**	**−2782**	4.3%
Stockholm	−1164	−1392	**−1397**	1%

Table 2
Q^2 indicator value for model checking. Q^2 for quantile plots on Gumbel scale is evaluated for large quantiles above 2. Q^2 for probability plots on Gumbel scale is evaluated for large probabilities above 80%.

Tide gauge	Selected model	Q^2 – residual quantile plot	Q^2 – residual probability plot
Brest	GEV2	0.972	0.978
Cuxhaven	GEV2	0.963	0.964
Gedser	GEV2	0.984	0.991
Halifax	GEV3	0.911	0.959
Honolulu	GEV3	0.837	0.968
Newlyn	GEV3	0.867	0.972
San Francisco	GEV2	0.968	0.996
Stockholm	GEV3	0.987	0.996

(Fig. 9), San Francisco, Halifax, Newlyn and Stockholm (at Cuxhaven, the partial effect NAO-μ is quasi linear; see Fig. 6b). These partial effects can be assimilated to quasi-bilinear functions, i.e. two regimes can be identified, a first monotonic quasi-linear regime, and a second quasi-constant one; see in particular Fig. 8e. The non-linear effect appears to mainly concern the remote influence of *CI* on σ (i.e. AMO at San Francisco, NINO12 and SOI at Halifax and Stockholm), on μ (NINO12 at Stockholm), and on ξ (SOI at Newlyn). The case of Newlyn appears to be particularly complex with two *CIs* acting on the tail behaviour with a Gumbel regime for moderate absolute value SOI (Fig. 9e) not larger than 1.0 and a switch from a Weibull (bounded) to a Fréchet (unbounded) regime for high AMO values above 0.1 (Fig. 9d). The derivation of these effects is however difficult and the confidence can only be considered high over specific range of *CI* values; see for instance at Stockholm (Fig. 9c) and at Newlyn (Fig. 9f), the degree of uncertainty prevents any confident analysis for SOI above 2, and over the interval [-1;1] respectively.

Regarding research question Q2 (can multiple *CI* influence extremes?), the answer is not systematic and depends on the considered tide gauge. Considering only partial effects associated with high confidence, we show that: at least one *CI* is integrated in the GEV formulation at Cuxhaven (NAO); at least two at Gedser (AMO and NAO); at least three at San Francisco (AMO, NINO12 and SOI) and Halifax (AMO, NAO,

	Brest (FR)	Cuxhaven (DE)	Gedser (DK)	Halifax (CA)	Honolulu (US)	Newlyn (UK)	San Francisco (US)	Stockholm (SW)
mu.AMO	-	-	L-	-	-	-	-	-
mu.NAO	L-	NL	L-	L-	-	L-	-	L+
mu.NINO12	-	-	-	-	L-	-	-	NL
mu.SOI	-	L-	-	L+	-	-	L-	-
scale.AMO	-	-	-	L+	L-	-	NL	L-
scale.NAO	-	L+	L-	-	L-	L-	-	-
scale.NINO12	L-	L-	-	NL	-	L-	L+	-
scale.SOI	-	L-	-	-	-	-	-	NL
shape.AMO	-	-	-	-	L-	NL	-	L+
shape.NAO	-	-	-	-	L+	-	-	-
shape.NINO12	-	-	-	L+	L-	L-	-	-
shape.SOI	-	-	-	-	L+	NL	-	-

Fig. 8. Types of partial effects at each tide gauge considering the different *CIs*. In purple: non-linear partial effects denoted NL; in green, linear decreasing denoted L-; in red, linear increasing denoted L+. The symbol "-" indicates that the procedure (either based on the analysis of AIC-LRT or on the penalization approach) has identified the considered covariate as of negligible influence. The light colours indicate that the relation is weak because of too high uncertainty. (For interpretation of the references to colour in this figure legend, the reader is referred to the Web version of this article.)

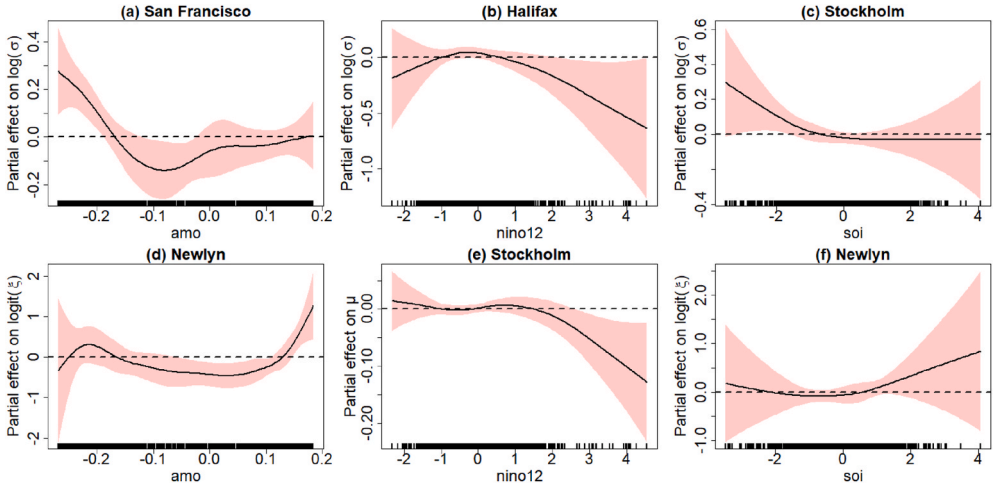

Fig. 9. Non-linear partial effects at San Francisco (a), Halifax (b), Stockholm (c,e), Newlyn (d,f).

and NINO12), and the four *CIs* at Newlyn and Stockholm.

Regarding Q3 (is the influence only on μ or is there any influence on the other GEV parameters?), the inspection of the partial effects confirms the results of the AIC-based analysis (completed by the LRT), i.e. the influence of *CIs* cannot be restricted to μ. At the exception of Gedser, all tide gauges present an influence either on μ-σ (Cuxhaven, San Francisco and Halifax) or on the three GEV parameters (Stockholm and Newlyn) altogether.

5. Discussion

While it is generally considered that projected changes in ESLs will be mostly driven by MSL changes, there remain questions regarding potential changes of ESLs induced by changing pressures and winds caused by climate change (Vousdoukas et al., 2018; Oppenheimer et al., 2019). Using a spline-based non-stationary extreme value analysis, we confirm the links between teleconnection patterns (modelled by *CIs*) and local ESLs, which have been previously identified in the literature using other methods. Several aspects deserve however further discussions, namely the relation between the *CIs* and the tide gauge's location (Sect. 5.1), the effect of seasonality of *CIs* (Sect. 5.2) and the limitations of our study (Sect. 5.3).

5.1. Relation between CI and tide gauge's location

Among the *CIs* identified with confidence, some are consistent with the spatial location of the considered tide gauge: NAO mainly influences the tide gauges located on the North Atlantic basin, either in Europe (Cuxhaven, Gedser, Newlyn, Stockholm), which is consistent with previous studies like Chafik et al. (2017) (see also Han et al. (2017) for a review), or in North American East Coast (Halifax), which is consistent with findings of Xu et al. (2019). Halifax tide gauge also includes a significant AMO signal (see Fig. B3.2), which appears to be consistent with the significant correlation found between AMO and sea-level anomaly in the North Atlantic subpolar region reported by Xu et al. (2019). Although less pronounced than for NAO, statistically significant AMO influences in some GEV parameters for European tides gauges records (see Supplementary Materials: Gedser, Fig. B2; Newlyn, Fig. B5; Stockholm, Fig. B7) are found. This result contrasts with the findings of Karabil et al. (2017), who conclude that, in the Baltics Sea region, no significant contribution of AMO-related factors to decadal sea-level could be found in historical tide gauges records. While further analyses would be needed to decipher this apparent contradiction (this goes beyond the scope of this paper), the comparison above underlines the relevance and added value of our method to investigate link between extreme sea levels and climate variability.

As expected, NINO12 and SOI have significant influences at tide gauges located in the Pacific basin (at San Francisco and with a higher

uncertainty at Honolulu). In addition, we note some teleconnection influence with mainly non-linear effects (Fig. 8): NINO12 and SOI appear to affect the North Atlantic coastal sea level (Newlyn, Stockholm and Halifax), and AMO appears to affect San Francisco. Teleconnections between ENSO and the North Atlantic-European have long been established (Brönnimann, 2007) and operate via several pathways that can imply e.g. the North Pacific area, the tropical Atlantic, or the stratosphere (Domeisen et al., 2019) through complex mechanisms. Teleconnections - although less well apprized - between the AMO and the North Pacific or tropical Pacific regions have been also reported (Wang, 2019), which appears consistent with the fact that AMO signatures are found in San Francisco records. These result suggest that our approach is suitable to identify complex relationships between local sea levels and remote large scale climate oscillations.

5.2. Effect of seasonality

The study has been performed by analysing the monthly SL maxima (after removal of the annual median) for all seasons by following a continuous time series analysis. Seasonality was accounted for by adding a seasonal functional term to describe the partial effect of the GEV parameters (Sect. 3.2). Due to the importance of seasonality in extremes (as previously outlined by Menéndez and Woodworth, 2010; Marcos and Woodworth, 2017), we further investigate this effect by re-conducting the analysis for the winter season, December-January-February (DJF), i.e. months at which seasonal partial effects of μ and/or for σ reach maxima (see Fig. 5 for Cuxhaven; and Supplementary Materials E for the other tide gauges).

Fig. 10 shows that the linear influence of some *CIs* is persistent when focusing on DJF and these signals even got strengthened (i.e. with lower uncertainty band) like for the SOI influence on σ at San Francisco, the NAO influence on μ at Cuxhaven, and the NINO12 influence on σ at Newlyn (the corresponding partial effects are provided in Supplementary Materials F). Signals with increasing confidence also emerge at some locations like at Honolulu: the DJF analysis clearly identifies strong NINO12 and AMO influences (compared to the weak *CI* influence in Fig. 8). At Newlyn, the signal also restricts to a few influences with AMO and NINO12 signal being strong. At Brest, the *CI* influence remains however unclear.

The non-linear signals are also unevenly affected when restricting our analysis to DJF. Some non-linear signals tend to remain persistent - e.g. AMO at Newlyn and SOI at Stockholm show quasi similar shape than those identified when the continuous time series are considered; see Supplementary Materials F - while others become more linear (e.g. AMO at San Francisco; NAO at Cuxhaven). Finally, some non-linear signals vanish for the months DJF and some become highly uncertain (NINO12 at Halifax, SOI at Newlyn, NINO12 at Stockholm on μ).

A complex influence of NINO12 is also outlined. Some teleconnections are identified with a statistically significant and linear signal of NINO12 emerging at Gedser, and at Stockholm in DJF. Though we acknowledge that the physical processes associated with this signal are not fully understood, this finding appears consistent with the statistically significant relation between ESL and Niño3 index outlined by Menéndez and Woodworth (2010). The complexity of El Niño influence at these locations is also in line with the results by Rohmer and Le Cozannet (2019), though this study is restricted to high percentiles. At San Francisco, in contrast with the continuous time series analysis (Fig. 8), we note that NINO12 in DJF primarily alters μ instead of σ (the signal is now of higher uncertainty), i.e. it drives the shift of the whole probability distribution instead of the dispersion (as illustrated by Fig. 1).

This type of analysis is useful to confirm the significance of some signals that were identified using the continuous time series, i.e. the monthly SL maxima for all seasons (Fig. 8); hence showing the robustness of the approach. This also shows the flexibility of the approach by highlighting complementary elements regarding teleconnections, though these should be further explored to unravel the underlying physical processes. This also opens the possibility for a deeper analysis of the *CI* influence at different seasons by accounting for the complexity of the seasonal partial effects at the different locations (Supplementary Materials E).

5.3. Limitations

Though significant signals have been identified, the non-negligible effect of the fitting uncertainty should be underlined (16 partial effects are identified with too high uncertainty to draw firm conclusions), even when using quasi century-long time series of SL. Deriving partial effects with high confidence is tedious for σ (as indicated by the number of cases in light colours in Fig. 8) and even more for ξ. This also goes in the same direction of the commonly-used and pragmatic assumption of keeping this ξ parameter constant. Methods within the Bayesian framework (Umlauf et al., 2018) is a promising solution in order to get a broader picture on the uncertainty at all levels of the approach (parameter fitting, data, structural uncertainty, etc.). Using the approach of Bayesian model averaging, Wong (2018) showed the interest of this framework by avoiding the model selection, which is a difficult task. Besides, this framework would give the opportunity to incorporate many sites in the analysis (instead of restricting to a single location), through a proper modelling of the spatial correlation between the sites (see e.g. Calafat and Marcos, 2020).

An alternative approach to analyse the links between climate

	Brest (FR)	Cuxhaven (DE)	Gedser (DK)	Halifax (CA)	Honolulu (US)	Newlyn (UK)	San Francisco (US)	Stockholm (SW)
mu.AMO	-	-	-	-	-	-	-	-
mu.NAO	-	L+	-	L-	-	-	L-	L+
mu.NINO12	L+	L-	L-	-	L-	-	NL	L-
mu.SOI	-	-	L-	-	-	-	L-	-
scale.AMO	-	-	-	-	L-	-	L-	L-
scale.NAO	-	L+	-	-	-	-	-	-
scale.NINO12	-	-	L+	L-	-	L-	L+	L+
scale.SOI	L+	-	-	-	L-	-	-	NL
shape.AMO	-	-	-	-	-	NL	L+	-
shape.NAO	-	-	-	-	-	-	L+	-
shape.NINO12	-	-	-	-	-	-	-	-
shape.SOI	-	-	-	-	-	L+	L+	-

Fig. 10. Types of partial effects at each tide gauge considering the different *CIs* by restricting the analysis to December-January-February. In purple: non-linear partial effects denoted NL; in green, linear decreasing denoted L-; in red, linear increasing denoted L+. The symbol "-" indicates that the procedure has identified the considered covariate as of negligible influence. The light colours indicate that the relation is weak because of too high uncertainty. (For interpretation of the references to colour in this figure legend, the reader is referred to the Web version of this article.)

variability and ESLs could rely on weather-type approaches consisting in classifying the typical regional climate settings that cause specific sea-level extremes may be more appropriate (e.g., Rueda et al., 2016). However, the regional weather types that emerge from such analysis are more difficult to interpret, as they are specific to each site considered. The approach consisting in assessing the links between teleconnection patterns with local water levels has the advantage that the modes of variability of teleconnection patterns and their links with storminess have been extensively studies (e.g., Seierstad et al., 2007). Hence, we argue that both approaches are required to progress in our understanding of present-day and future sea-level extremes.

6. Summary and further works

Using a spline-based non-stationary formulation of GEV, we provide new insight into the links between extreme local sea levels and teleconnection patterns. First, the links between the climate indices and different parameters of a GEV distribution fitted to extreme sea-level data are shown to be most of the time linear (research question Q1), but some of them present significant non-linear forms, as shown for instance in Halifax, San Francisco, Stockholm, and Honolulu, as well as at Cuxhaven to a lesser extent. To our best knowledge, taking into account these non-linear effects has rarely been done in previous studies at the exception of Wong (2018) but by assuming a second-order polynomial relation between the GEV parameters and the *CI*s. Including more complex functional relationships can have strong impacts for probabilistic flooding risk assessments and preparedness to flood events, since the time evolution of GEV parameters directly affects the one of return levels, and potentially its future projections. Furthermore, we show that multiple climate indices should be considered to predict extreme sea-levels (research question Q2), and that the influence of climate indices of the GEV distribution is not limited to the location parameter μ (research question Q3), but can also affect the scale and shape parameters σ and ξ, as shown at multiple coastal sites either in Europe (Newlyn, and Stockholm), in North America (Halifax) or in Pacific (San-Francisco). The results presented here are a step forward to reducing uncertainties in extreme sea-level analysis, and can be useful to reduce the risks of under- or over-adaptation to storms (e.g., Hall et al., 2012). As another perspective, this type of research may also help improving our understanding of potential links between climate variability and storms and support preparedness to unusual sequence of storms driven by the persistence of specific climate conditions (e.g., see Castelle et al., 2017).

Different lines of further research can be followed. First, we followed common practices used in literature to model MSL via the annual median value as described in Sect. 2. This aspect could be improved by taking advantages of more advanced statistical techniques like Kalman-filter as applied by Rohmer and Le Cozannet (2019). Second, the choice of *CI*s should be improved. Considering alternative *CI*s is an option (for instance NINO34 instead of NINO12, see the correlation analysis in Supplementary Material C), or "tailored" *CI* specifically developed for the purpose of SL variability study as Wahl and Chambers (2016) did in the US, or Dangendorf et al. (2014) in the German Bight. The major unresolved problem is to account for dependencies among *CI*s. Using bivariate formulation of splines may here be beneficial (see an example for lightning prediction by Simon et al. (2019)). Third, climate variability is not the only factor affecting ESL and additional physical processes may significantly act. This is indicated by the statistically significant linear coefficients of the long term trend at some stations (Supplementary Materials D). Attributing this signal to physical processes deserves further investigations; such processes may include effects of river flows (in estuaries, see e.g., Piecuch et al., 2018), evolving complex nonlinear shallow water processes (see a comprehensive review by Woodworth et al., 2019), and nonlinear vertical ground motions (e.g., Raucoules et al., 2013), among others. Finally, it should be noted that we investigated the covariates' influence by assuming a co-occurrence with the monthly SL maxima. As a line for future research, lagged effects are also worth investigating by extending, for instance, the study by Andrew et al. (2006) to extremes.

The proposed framework is here flexible enough to integrate additional covariates. The penalization-based variable selection can here show its benefits.

CRediT authorship contribution statement

Jérémy Rohmer: Conceptualization, Data curation, Formal analysis, Investigation, Methodology, Software, Supervision, Visualization, Writing – original draft, Writing – review & editing. **Rémi Thieblemont:** Data curation, Formal analysis, Investigation, Visualization, Writing – review & editing. **Gonéri Le Cozannet:** Formal analysis, Investigation, Visualization, Writing – review & editing, Funding acquisition.

Declaration of competing interest

The authors declare that they have no known competing financial interests or personal relationships that could have appeared to influence the work reported in this paper.

Acknowledgements

We acknowledge financial support of ARN Storisk project (ANR-15-CE03-0003) and of INSeaPTION project, which is part of ERA4CS, an ERA-NET initiated by JPI Climate and co-funded by the European Union (Grant #690462). The first author also acknowledges financial support of EUPHEME project, which is also part of ERA4CS. We are grateful to Prof. Philip Jonathan (Lancaster uni.) for his inspiring talk at EVAN 2019 conference which motivated the finalisation of this study. The implementation was carried out using the R package mgcv (https://cran.r-project.org/web/packages/mgcv/index.html). The R scripts are available from the author upon request.

Appendix A. Supplementary data

Supplementary data to this article can be found online at https://doi.org/10.1016/j.wace.2021.100352.

References

Akaike, H., 1998. Information theory and an extension of the maximum likelihood principle. In: Selected Papers of Hirotugu Akaike. Springer, New York, pp. 199–213.
Andrew, J.A., Leach, H., Woodworth, P.L., 2006. The relationships between tropical Atlantic sea level variability and major climate indices. Ocean Dynam. 56 (5–6), 452–463.
Becker, M., Karpytchev, M., Lennartz-Sassinek, S., 2014. Long-term sea level trends: natural or anthropogenic? Geophys. Res. Lett. 41 (15), 5571–5580.
Beirlant, J., Goegebeur, Y., Segers, J., Teugels, J., 2004. Statistics of Extremes: Theory and Applications. Wiley & Sons, Chichester, UK.
Burnham, K.P., Anderson, D.R., 2004. Multimodel inference: understanding AIC and BIC in model selection. Socio. Methods Res. 33 (2), 261–304.
Brönnimann, S., 2007. Impact of El Niño–Southern oscillation on European climate. Rev. Geophys. 45, RG3003.
Calafat, F.M., Chambers, D.P., Tsimplis, M.N., 2012. Mechanisms of decadal sea level variability in the eastern North Atlantic and the Mediterranean Sea. J. Geophys. Res.: Oceans 117 (C9).
Calafat, F.M., Marcos, M., 2020. Probabilistic reanalysis of storm surge extremes in Europe. Proc. Natl. Acad. Sci. Unit. States Am. 117 (4), 1877–188.
Castelle, B., Dodet, G., Masselink, G., Scott, T., 2017. A new climate index controlling winter wave activity along the Atlantic coast of Europe: the West Europe Pressure Anomaly. Geophys. Res. Lett. 44 (3), 1384–1392.
Ceres, R.L., Forest, C.E., Keller, K., 2017. Understanding the detectability of potential changes to the 100-year peak storm surge. Climatic Change 145 (1–2), 221–235.
Chafik, L., Nilsen, J.E.Ø., Dangendorf, S., 2017. Impact of North Atlantic teleconnection patterns on Northern European sea level. J. Mar. Sci. Eng. 5 (3), 43.
Chang, Y.-T., Du, L., Zhang, S.-W., Huang, P.-F., 2013. Sea level variations in the tropical Pacific Ocean during two types of recent El Niño events. Global Planet. Change 108, 119–127.
Cheng, L., AghaKouchak, A., Gilleland, E., Katz, R.W., 2014. Non-stationary extreme value analysis in a changing climate. Climatic Change 127 (2), 353–369.

Coles, S.G., 2001. An introduction to statistical modeling of extreme values, Springer series in statistics. Springer, London.
Dangendorf, S., Wahl, T., Nilson, E., Klein, B., Jensen, J., 2014. A new atmospheric proxy for sea level variability in the southeastern North Sea: observations and future ensemble projections. Clim. Dynam. 43, 447–467.
Domeisen, D.I.V., Garfinkel, C.I., Butler, A.H., 2019. The teleconnection of El Niño Southern oscillation to the stratosphere. Rev. Geophys. 57.
Frederikse, T., Buchanan, M.K., Lambert, E., Kopp, R.E., Oppenheimer, M., Rasmussen, D.J., van de Wal, R.S.W., 2020. Antarctic Ice Sheet and emission scenario controls on 21st-century extreme sea-level changes. Nat. Commun. 11 (390) https://doi.org/10.1038/s41467-019-140496.
Grinsted, A., Moore, J.C., Jevrejeva, S., 2013. Projected Atlantic hurricane surge threat from rising temperatures. Proc. Natl. Acad. Sci. Unit. States Am. 110, 5369–5373.
Han, W., Meehl, G.A., Stammer, D., Hu, A., Hamlington, B., Kenigson, J., Palanisamy, H., Thompson, P., 2017. Spatial patterns of sea level variability associated with natural internal climate modes. Surv. Geophys. 38, 217–250.
Hall, J.W., Brown, S., Nicholls, R.J., Pidgeon, N.F., Watson, R.T., 2012. Proportionate adaptation. Nat. Clim. Change 2, 833–834.
Han, W., Stammer, D., Thompson, P., et al., 2019. Impacts of Basin-Scale Climate Modes on Coastal Sea Level: a Review. Surv Geophys 40, 1493–1541. https://doi.org/10.1007/s10712-019-09562-8.
Höge, M., Wöhling, T., Nowak, W., 2018. A primer for model selection: the decisive role of model complexity. Water Resour. Res. 54 (3), 1688–1715.
Hurrell, J.W., Kushnir, Y., Visbeck, M., Ottersen, G., 2003. In: Hurrell, J.W., Kushnir, Y., Ottersen, G., Visbeck, M. (Eds.), An Overview of the North Atlantic Oscillation, The North Atlantic Oscillation, Climatic Significance and Environmental Impact, vol. 134. AGU Geophysical Monograph, pp. 1–35.
Karabil, S., Zorita, E., Hünicke, B., 2017. Mechanisms of variability in decadal sea-level trends in the Baltic Sea over the 20th century. Earth Syst. Dynam. 8, 1031–1046.
Kim, H., Kim, S., Shin, H., Heo, J.H., 2017. Appropriate model selection methods for nonstationary generalized extreme value models. J. Hydrol. 547, 557–574.
Kundzewicz, Z.W., Szwed, M., Pińskwar, I., 2019. Climate variability and floods—a global review. Water 11 (7), 1399. https://doi.org/10.3390/w11071399.
Lang, A., Mikolajewicz, U., 2019. The long-term variability of extreme sea levels in the German Bight. Ocean Sci. 15 (3), 651–668.
Marcos, M., Calafat, F.M., Berihuete, Á., Dangendorf, S., 2015. Long-term variations in global sea level extremes. J. Geophys. Res. 120 (12), 8115–8134.
Marcos, M., Woodworth, P.L., 2017. Spatiotemporal changes in extreme sea levels along the coasts of the North Atlantic and the Gulf of Mexico. J. Geophys. Res. 122 (9), 7031–7048.
Marra, G., Wood, S.N., 2011. Practical variable selection for generalized additive models. Computational Statistics & Data Analysis 55 (7), 2372–2387.
Mawdsley, R.J., Haigh, I.D., 2016. Spatial and temporal variability and long-term trends in skew surges globally. Front. Mar. Sci. 3 (29) https://doi.org/10.3389/fmars.2016.00029.
Méndez, F.J., Menéndez, M., Luceño, A., Losada, I.J., 2007. Analyzing monthly extreme sea levels with a time-dependent GEV model. J. Atmos. Ocean. Technol. 24 (5), 894–911.
Menéndez, M., Woodworth, P.L., 2010. Changes in extreme high water levels based on a quasi-global tide-gauge dataset. J. Geophys. Res. 115, C10011. https://doi.org/10.1029/2009JC005997.
Merrifield, M., Kilonsky, B., Nakahara, S., 1999. Interannual sea level changes in the tropical Pacific associated with ENSO. Geophys. Res. Lett. 26, 3317–3320.
Muis, S., Haigh, I.D., Guimarães Nobre, G., Aerts, J.C., Ward, P.J., 2018. Influence of El Niño-Southern oscillation on global coastal flooding. Earth's Future 6 (9), 1311–1322.
Nicholls, R.J., Cazenave, A., 2010. sea level rise and its impact on coastal zones. Science 328, 1517–1520.
Oppenheimer, M., Glacovic, B., Hinkel, J., Van De Wal, R., Magnan, A., Abd-Elgawad, A., Cai, R., Cifuentes-Jara, M., Deconto, R., Ghosh, T., Hay, J., Isla, F., Marzeion, B., Meyssignac, M., Sebesvari, Z., 2019. sea-level rise and implications for low Lying islands, coasts and communities, special report on the ocean and cryosphere in a changing climate (SROCC) (in press). available at: https://report.ipcc.ch/srocc/pdf/SROCC_FinalDraft_Chapter4.pdf.
Piecuch, C.G., Bittermann, K., Kemp, A.C., Ponte, R.M., Little, C.M., Engelhart, S.E., Lentz, S.J., 2018. River-discharge effects on United States Atlantic and Gulf coast sea-level changes. Proc. Natl. Acad. Sci. Unit. States Am. 115 (30), 7729–7734.
Rashid, M.M., Wahl, T., 2020. Predictability of extreme sea level variations along the US coastline. J. Geophys. Res.: Oceans 125 (9), e2020JC016295.
Raucoules, D., Le Cozannet, G., Wöppelmann, G., De Michele, M., Gravelle, M., Daag, A., Marcos, M., 2013. High nonlinear urban ground motion in Manila (Philippines) from 1993 to 2010 observed by DInSAR: implications for sea-level measurement. Remote sensing of environment 139, 386–397.
Rigby, R.A., Stasinopoulos, D.M., 2005. Generalized additive models for location, scale and shape. J. Roy. Stat. Soc: Series C (Appl. Stat.) 54 (3), 507–554. https://doi.org/10.1111/j.1467-9876.2005.00510.x.
Rohmer, J., Le Cozannet, G., 2019. Dominance of the mean sea level in the high-percentile sea levels time evolution with respect to large-scale climate variability: a Bayesian statistical approach. Environ. Res. Lett. 14 https://doi.org/10.1088/1748-9326/aaf0cd.
Rueda, A., Camus, P., Tomás, A., Vitousek, S., Méndez, F.J., 2016. A multivariate extreme wave and storm surge climate emulator based on weather patterns. Ocean Model. 104, 242–251.
Salas, J.D., Obeysekera, J., 2014. Revisiting the concepts of return period and risk for nonstationary hydrologic extreme events. J. Hydrol. Eng. 19, 554–568.
Schwarz, G., 1978. Estimating the dimension of a model. Ann. Stat. 6, 461–464.
Seierstad, I.A., Stephenson, D.B., Kvamstø, N.G., 2007. How useful are teleconnection patterns for explaining variability in extra-tropical storminess? Tellus Series A-Dynam. Meteorol. Oceanogr. 59 (2), 170–181.
Simon, T., Mayr, G.J., Umlauf, N., Zeileis, A., 2019. NWP-based lightning prediction using flexible count data regression. Adv. Stat. Climatol. Meteorol. Oceanogr. 5 (1), 1–16.
Talke, S.A., Orton, P., Jay, D.A., 2014. Increasing storm tides in New York Harbor, 1844–2013. Geophys. Res. Lett. 41, 3149–3155. https://doi.org/10.1002/2014GL059574.
Umlauf, N., Klein, N., Zeileis, A., 2018. BAMLSS: bayesian additive models for location, scale and shape (and beyond). J. Comput. Graph Stat. 27 (3), 612–627.
Vousdoukas, M.I., Mentaschi, L., Voukouvalas, E., Verlaan, M., Jevrejeva, S., Jackson, L. P., Feyen, L., 2018. Global probabilistic projections of extreme sea levels show intensification of coastal flood hazard. Nat. Commun. 9 (1), 1–12.
Wahl, T., 2017. Sea-level rise and storm surges, relationship status: complicated! Environ. Res. Lett. 12 (11), 111001. https://doi.org/10.1088/1748-9326/aa8eba.
Wahl, T., Chambers, D.P., 2015. Evidence for multidecadal variability in US extreme sea level records. J. Geophys. Res. 120, 1527–1544.
Wahl, T., Chambers, D.P., 2016. Climate controls multidecadal variability in US extreme sea level records. J. Geophys. Res. 121 (2), 1274–1290.
Wang, C., 2019. Three-ocean interactions and climate variability: a review and perspective. Clim. Dynam. 53 (7–8), 5119–5136.
Wong, T.E., 2018. An integration and assessment of multiple covariates of nonstationary storm surge statistical behavior by bayesian model averaging. Adv. Stat. Climatol. Meteorol. Oceanogr. 4, 53–63.
Wong, T.E., Klufas, A., Srikrishnan, V., Keller, K., 2018. Neglecting model structural uncertainty underestimates upper tails of flood hazard. Environ. Res. Lett. 13 (7), 074019 https://doi.org/10.1088/1748-9326/aacb3d.
Wood, S.N., 2017. Generalized Additive Models: an Introduction with R, second ed. Chapman and Hall/CRC, Boca Raton, Florida.
Wood, S.N., Pya, N., Säfken, B., 2016. Smoothing parameter and model selection for general smooth models. J. Am. Stat. Assoc. 111 (516), 1548–1563, 2016.
Wood, S.N., 2003. Thin-plate regression splines. J. Roy. Stat. Soc. 65, 95–114.
Woodworth, P.L., Melet, A., Marcos, M., Ray, R.D., Wöppelmann, G., Sasaki, Y.N., Cirano, M., Hibbert, A., Huthnance, J.M., Monserrat, S., Merrifield, M.A., 2019. Forcing factors affecting sea level changes at the coast. Surv. Geophys. 40 (6), 1351–1397.
Woodworth, P.L., Hunter, J.R., Marcos, M., Caldwell, P., Menendez, M., Haigh, I., 2016. Towards a global higher-frequency sea level data set. Geosci. Data J. 3, 50–59.
Woodworth, P.L., Menéndez, M., Gehrels, W.R., 2011. Evidence for century-timescale acceleration in mean sea levels and for recent changes in extreme sea levels. Surv. Geophys. 32 (4–5), 603–618.
Xu, Q., Tu, K., Cheng, Y., Wang, W., Jia, Y., Ye, X., 2019. Satellite altimetry and tide gauge observed teleconnections between long-term sea level variability in the US East Coast and the North Atlantic ocean. Rem. Sens. 11 (23), 2816. https://doi.org/10.3390/rs11232816.